Journal of Molecular Liquids 416 (2024) 126485

Contents lists available at ScienceDirect

Journal of Molecular Liquids

journal homepage: www.elsevier.com/locate/molliq

Effect of p-toluidine hydrochloride on the phase behavior of aqueous solution of sodium dodecyl sulfate

Mukesh Chandra Bos [a], Shallu Dhingra [b], Manoj Kumar Srivastava [c], Pawan Kumar [a], Divesh Kumar [a], Santanu Kumar Pal [b,*], Santosh Prasad Gupta [a,*]

[a] Department of Physics, Patna University, Patna, 800005, Bihar, India
[b] Department of Chemical Sciences, Indian Institute of Science Education and Research (IISER) Mohali, Sector-81, SAS Nagar, Knowledge City, Manauli, Mohali, 140306, Punjab, India
[c] Department of Physics, D. A. V. P. G. College, Gorakhpur, 273001, U. P., India

ARTICLE INFO

Keywords:
SDS
PTHC
H phase
L_α phase
L_x phase

ABSTRACT

We have investigated the effects of an organic salt, namely p-toluidine hydrochloride (PTHC), on the phase behavior of aqueous solutions of an anionic surfactant, sodium dodecyl sulfate (SDS). Specially, the behavior of SDS-PTHC-water system at 40 °C has been studied using small angle X-ray scattering (SAXS) and polarizing optical microscopy (POM) techniques. As the concentration of PTHC increases, the system exhibits three phases, namely: hexagonal (H), a lamellar (L_α) phase with excessive water, denoted by ($I + L_\alpha$), and an isotropic phase of bilayer (L_x) with excess water, symbolized by ($I + L_x$). Electron density maps has been reconstructed for the H and L_α phases. The L_α phase and the L_x phase are both found to be satisfactorily represented by the model of the L_α phase. It is apparent from the findings that a substantial quantity of organic salts can be utilized to screen out the ionic charges of the surfactant and stabilize the L_x phase.

1. Introduction

Amphiphile and surfactant are sometimes used interchangeably because surfactants are common examples of amphiphiles. Amphiphilic compounds are frequently comprised of two or more moieties with distinct properties, such as hydrophilic and hydrophobic. The charge of the hydrophilic group determines the classification of surfactants as either nonionic or ionic (anionic and cationic). The hydrophilic groups that make up anionic surfactants typically contain carboxylate, sulfate, phosphate, and sulphonate. The main constituents of cationic surfactants are nitrogen-containing quaternary compounds that have positive charges. Cetyltrimethylammonium bromide (CTAB) is the most popular cationic surfactant, and sodium dodecyl sulfate (SDS) is another popular anionic surfactant [1–3].

The amphiphilic nature of surfactant molecules in an aqueous solution causes them to form a variety of unique aggregates (micelles) of different shapes above the critical micellar concentration (CMC) [4,5]. The assembly of amphiphiles is crucial for various applications, including food, cosmetic, and pharmaceutical formulations. Amphiphilic self-assembling peptides have been frequently used in tissue and cell engineering, antimicrobials, drug delivery systems, and other biomedical applications because of their outstanding biocompatibility [6–8].

The shape of these self-assembled aggregates are determined by the amphiphile itself, which is often expressed in terms of the shape parameter $p = v/al$, where l represents the average chain length in the aggregate, a denotes the ideal head group area, and v represents the hydrocarbon chain volume of the amphiphile [1,8,9]. For a surfactant with a bulky head and a single chain, the preferred shape of micelles is spherical with $p \sim \frac{1}{3}$. The surfactant with a single chain and a moderate head group produces cylindrical micelles, despite the fact that it provides the value of $p \sim \frac{1}{2}$. Additionally, amphiphiles with p~1, which comprise the majority of bio-membrane components, form bilayers in diluted solutions. Moreover, it is the preferred aggregation form in 'catanionic' systems, which are combinations of anionic and cationic single-tailed amphiphiles. In this catanionic system, bilayers appear in the form of unilamellar vesicles (ULVs) when the composition of the constituted amphiphiles is close to equimolar [10].

Organic salts, such as 2-sodium-3-hydroxy naphthoate (SHN) and p-toluidine hydrochloride (PTHC), are not able to form micelles on their own in water. However, in the presence of amphiphile, they choose to

* Corresponding author.
E-mail addresses: skpal@iisermohali.ac.in, santanupal.20@gmail.com (S.K. Pal), santosh-phy@patnauniversity.ac.in, drspgpu@gmail.com (S.P. Gupta).

https://doi.org/10.1016/j.molliq.2024.126485
Received 2 July 2024; Received in revised form 12 October 2024; Accepted 10 November 2024
Available online 14 November 2024

sit at the surface of the micelle and consequently affect the properties of the micelle-water interface, this makes them an extreme example of an ionic amphiphile [9,11–13]. These molecules, commonly known as hydrotropes, play a crucial role in mitigating the spontaneous curvature of the micelle surface. In numerous amphiphiles, this reduction is sufficient to induce the formation of long, worm-like micelles (WLM), as evidenced by studies, as listed in the references [9,11]. Furthermore, bilayers have been observed to stabilize under certain conditions, particularly when there is a notable reduction in the spontaneous curvature [9,11,13].

A common phase that emerges from bilayers is the lamellar phase, characterized by the stacking of bilayers in a periodic manner on top of each other [8]. The lamellar periodicity (d) of these systems, when devoid of osmotic pressure, is determined by the balance of various inter-bilayer interactions. These interactions encompass steric repulsion, van der Waals attraction, electrostatic repulsion, and hydration repulsion [1]. Furthermore, the short-range hydration force is the result of the ordered arrangement of water molecules at the bilayer surface, coupled with the extrusion of molecules beyond the bilayer due to thermal agitation, while the steric repulsion arises from the thermal fluctuations of the bilayer structures [14].

Bilayers are also capable of exhibiting isotropic phases, such as the sponge (L_3) phase, and the dispersion of uni-lamellar vesicles (ULVs), devoid of any long-range positional or orientational order [15]. The L_3 phase has been observed in certain highly diluted amphiphilic systems, characterized by a random network of bilayers, and manifests alongside the presence of inorganic salts (e.g., NaCl) or cosurfactants (e.g., short-chain alcohols) [16–18]. The cosurfactant enhances the flexibility of the bilayer network, whereas the salt inhibits electrostatic interactions, consequently, steric repulsion prevails in interactions between bilayers.

Although the L_3 phase is primarily characterized by steric repulsion, there has been a recent discovery of a novel variant known as the "L_x" phase in several systems, which is predominantly marked by attractive interactions. This phase is distinguished by short-range positional correlations and small average inter-bilayer spacing, as evidenced by studies such as discussed in the references [19,20]. In these systems, the presence of salt screens out electrostatic interactions, while the short-range repulsive hydration interaction counteracts the attractive van der Waals forces, leading to a weakened swollen phase. Although it has been suggested that the L_x phase might form a bilayer network interconnected with one another, the precise structure of this phase remains enigmatic.

The anionic surfactant, SDS, has been the focus of extensive research, leading to the identification of several intermediate phases within its system, including ribbon, ordered mesh, bicontinuous cubic, and hexagonal (H) phases, as well as lamellar (L_α) phases. However, these phases are predominantly observed within a narrow range of compositions [21]. Previous investigations have examined the phase behavior of the SDS-PTHC-water system, revealing that at high salt concentrations, both the L_α and an isotropic phase denoted by L_3 phases coexist with excess water [supporting Figure S1]. The corresponding small angle X-ray scattering (SAXS) pattern shows a narrow peak associated with the L_α phase, conversely, the L_3 phase presents a broader peak in the diffraction pattern [22]. Analysis indicates that the positions of the peaks for the L_α and L_3 phases are nearly identical [supporting Figure S1]. It is recognized that the L_3 phase, although not explicitly identified in the preceding literature, exhibits distinct characteristics when compared to the previously discussed L_3 phase. The detailed structural features of this particular isotropic (which is denoted as L_3) phase, are currently undisclosed, and thus, this phase will henceforth be referred to as the L_x phase.

This article scrutinizes the influence of hydrotrope, PTHC, on the phase behavior of the anionic surfactant, SDS in aqueous media (SDS-PTHC-water system) at varying molar ratios of [PTHC]/[SDS] and at a constant concentration of SDS + PTHC in water ($\Phi_s = 50$) and fixed temperature ($T = 40°$ C). Polarizing optical microscopy (POM) and SAXS techniques are utilized to delineate the distinct phases exhibited by the SDS-PTHC-water system. The system presents a series of phases, identified as hexagonal (H), L_α, and L_x, that appear in response to increasing PTHC concentration. It has been observed that both the L_α and L_x phases coexist alongside excess water, resulting in distinct phases denoted as $I + L_\alpha$ and $I + L_x$, respectively. In this investigation, the L_α phase was modeled by adopting the methodology outlined by Pabst et al. [23], and it was found that this model adequately described the L_α phase, with a similar model demonstrating a high degree of applicability to the L_x phase. The document is structured like this: first, it describes the materials and methods used, then it presents the outcomes, and concludes with an in-depth analysis of the results.

2. Materials and methods

The organic salt, PTHC, and surfactant, SDS, were procured from Sigma-Aldrich and used without further purification, the chemical structure is shown in supporting [supporting Figure S2]. The addition of deionized water (Millipore) to the combination of surfactant-organic salt facilitated the creation of solutions, adjusting molar ratios ($\alpha = [PTHC]/[SDS]$) from 0 to 1.3 in increments of 0.1, while maintaining a fixed concentration of the solution ($\Phi_s = 50$), which was the total weight percentage of surfactant and organic salt dissolved in water. Subsequently, the samples were enclosed in tubes, sealed, and allowed to acclimate for a duration exceeding a week at a temperature of 40 °C.

For the purpose of POM observations under crossed polarizers, the samples were positioned between a glass slide and a cover slip. Textural observations of the mesophase were performed with Nikon Eclipse LV100POL Polarizing optical microscope (POM) provided with a Linkam heating stage (LTS 420). All images were captured using a Q-imaging camera. It was noted that phase changes were monitored only for the region closely to the center of the sample, away from its edges.

The samples were encased within glass capillaries (Hampton Research), each with a diameter of 0.7 mm, subsequently flame-sealed to facilitate the analysis through SAXS techniques. Upon the filling of these capillaries, it was observed that certain samples exhibited alignment due to shear flow. To generate the necessary X-ray radiation, a shield tube anode from a GeniX 3D X-ray generating Cu source (provided by Xenocs), equipped with a collimating multi-layer mirror, was utilized. This device operated at a voltage of 50 kV and a current of 0.6 mA was applied to produce diffraction patterns. The data from these patterns were captured using a two-dimensional Pilatus detector, characterized by a pixel size of 172 μm x 172 μm. The exposure times for each scan varied between 20 and 90 minutes. The precision with which the spacing of the small-angle sharp peak in the diffraction patterns could be measured was impressive, with an accuracy of 0.03 nm. Conversely, the determination of the spacing of the diffuse peaks was limited to an accuracy of 0.1 nm.

3. Results and discussion

The phase behavior of the SDS-PTHC-water system, at temperatures denoted as $T = 40$ °C, $\Phi_s = 50$, and varying values of α, is represented in figure [Fig. 1]. The existence of different phases at various compositions is confirmed through the examination of their SAXS patterns and POM textures. At lower α values, the system demonstrates the H phase. Furthermore, the L_α and L_x phases show stabilization at higher α values. However, it is observed that an excess of water coexists within the L_α and L_x phases, thus classifying these phases as $I + L_\alpha$ and $I + L_x$, respectively. The observed sequence of phase transitions is $H \rightarrow I + L_\alpha \rightarrow I + L_\alpha + L_x \rightarrow I + L_x$, demonstrating a progressive increase in α. A comprehensive analysis of this phase behavior is provided below.

The SDS-PTHC-water system exhibits a smooth texture under crossed POM at $\alpha = 0.0$, $\Phi_s = 50$ & $T = 40$ °C [Fig. 2A] and the associated SAXS pattern show two sharp peaks in the small angle region with d-spacing in the ratio $1 : \frac{1}{\sqrt{3}}$, which correspond to the reflections from the (100) and (110) planes of the two-dimensional hexagonal lattice, respectively [Fig. 3A (a)]. The d-spacings are calculated by using the relation $d_{hkl} =$

Table 1
Observed and calculated d-spacings, Miller indices, intensities, phases for the various phases exhibited by SDS-PTHC-water system at $\Phi_s = 50$ and $T = 40\,°C$.

α	Lattice Parameter (Å)	Miller indices (hkl)	d_{obs} (Å)	d_{cal} (Å)	Relative Intensity	Multi-plicity	$\Phi(hkl)$	Phase
0.0	47.25	(100)	40.92	40.92	100.00	6	π	H
		(110)	23.57	23.62	4.98	6	π	
0.1	51.11	(100)	44.26	44.26	100.00	6	π	H
		(110)	25.53	25.55	5.31	6	π	
0.2	41.26	(100)	41.26	41.26	100.00	2	π	$I + L_\alpha$
		(200)	20.67	20.63	1.48	2	π	
0.3	38.06	(100)	38.06	38.06	100.00	2	π	$I + L_\alpha$
		(200)	19.06	19.03	2.53	2	π	
0.4	38.32	(100)	38.32	38.32	100.00	2	π	$I + L_\alpha$
		(200)	19.29	19.16	2.95	2	π	
0.5	39.58	(100)	39.58	39.58	100.00	2	π	$I + L_\alpha$
		(200)	19.76	19.79	4.91	2	π	

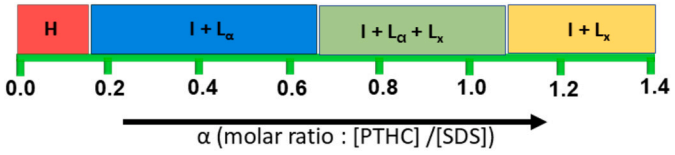

Fig. 1. Phase behavior of SDS-PTHC-water system at $T = 40\,°C$, $\Phi_s = 50$, and at various values of molar ratio, $\alpha = [PTHC]/[SDS]$. H, L_α, L_x and I denote hexagonal phase, lamellar phase, isotropic phase of bilayer and isotropic phase due to excess water, respectively.

$\frac{\sqrt{3}a}{2\sqrt{h^2+h\ k+k^2}}$. The calculated lattice parameter is found to be $a = 47.25$ Å [Table 1]. Moreover, the presence of a smooth POM texture supports the occurrence of the H phase which is made up of cylindrical micelles.

In a similar manner, the SDS-PTHC-water system demonstrates the H phase at $\alpha = 0.1$, $\Phi_s = 50$, and $T = 40\,°C$. The POM texture, however, exhibits a striated fan-like texture when observed under cross polarizers [Fig. 2B], indicating that cylindrical micelles transform into worm-like micelles upon the addition of PTHC to SDS. The arrangement of these worm-like micelles in a zigzag or undulating configuration, leading to these striations, can be observed in the optical length scale [24,25]. The existence of the H phase is further validated by the SAXS pattern, which reveals two peaks within the small angle region with a d-spacing in ratio of $1 : \frac{1}{\sqrt{3}}$, as evidenced in figure [Fig. 3A]. The aforementioned information is succinctly summarized in table [Table 1].

Furthermore, at $\alpha = 0.3$, $\Phi_s = 50$, at $T = 40\,°C$, the SDS-PTHC-water system displays an oily streak texture under crossed polarizers, accompanied by an optically isotropic region, indicative of the onset of the L_α phase [Fig. 2D]. The associated SAXS pattern reveals two distinct sharp peaks within the small angle region, with d-spacing in ratio of $1 : \frac{1}{2}$, corresponding to the reflections from the (100) and (200) planes, respectively, of the one-dimensional periodic lattice [Fig. 3B (b)]. This observation supports the occurrence of the L_α phase, however, it has been observed that the L_α phase coexists with excess water. The integration of results from the POM and SAXS studies confirms the presence of the L_α phase in coexistence with excess water, symbolized as $I + L_\alpha$, where I represents the isotropic phase facilitated by the excess water. The calculated lamellar periodicity has been determined to be $d = 38.06$ Å.

Moreover, under crossed polarizers, the SDS-PTHC-water system, when set at $\alpha = 0.2$, $\Phi = 50$, and $T = 40\,°C$, exhibits an oily streak texture [Fig. 2C]. Additionally, the corresponding SAXS pattern demonstrates the presence of two peaks in the small angle region [Fig. 3B (a)], with d-spacing in ratio of $1 : \frac{1}{2}$, further corroborating the existence of the $I + L_\alpha$ phase. Similarly, the SDS-PTHC-Water system, when set at $\alpha = 0.4$, $\alpha = 0.5$, $\alpha = 0.6$, $\Phi = 50$, and $T = 40\,°C$, also displays evidence of the $I + L_\alpha$ phase [Fig. 3B (c,d)]. The details of this phase behavior are summarized in table [Table 1].

Additionally, the SAXS pattern of the SDS-PTHC-water system, under conditions of $\alpha = 1.1$, $\alpha = 1.2$, $\alpha = 1.3$, $\Phi = 50$, and $T = 40\,°C$, reveals a single broad peak within the small angle region, characterized by a d-spacing of approximately 40 Å [Fig. 3D]. This value is notably close to, if not identical, to the d-spacing observed in the phase corresponding to the first peak of the L_α phase. Moreover, the phase exhibits optically isotropic behavior when viewed through crossed polarizers, yet it displays flow birefringence. The presence of flow birefringence, combined with the average spacing observed in this phase being near the periodicity of the L_α phase, suggests the composition of this phase consists of bilayer-like amphiphile aggregates and therefore, this phase is referred to as the isotropic phase of the bilayers (L_x). Additionally, it is noted that the sample contains an excess amount of water, thereby, the observed phase is referred to as '$I + L_x$'.

Additionally, the SAXS pattern of the SDS-PTHC-water system at α values ranging from 0.7 to 1.0, with $\Phi_s = 50$ and $T = 40\,°C$, displays a single peak within the small-angle region. This peak may be interpreted as the result of the convolution of two distinctly characterized peaks, one of which is narrow and the other broadly defined, indicative of the coexistence of the L_α phase which corresponds to the narrow peak, and the L_x phase, which is related to the broad peak [Fig. 3C & supporting Figure S3]. Moreover, the phase contains an excess of water, thereby leading to the observed phase to be represented by $I + L_\alpha + L_x$. A representative two-dimensional (2D) SAXS pattern of each of these phases (as discussed above) is further presented in the supporting figures [supporting Figure S4].

We have determined the correlation length to gain insights into the order of the observed phases. The formula $\xi = \frac{2\pi k}{\Delta q}$ is utilized to calculate the correlation length, which corresponds to the extent of order within mesophases. This equation is analogous to Scherrer's formula, $\xi = \frac{\lambda k}{\Delta(2\theta)Cos\theta}$, where θ represents the position of the peak in radians, λ denotes the wavelength of the incident X-ray, $\Delta(2\theta)$ characterizes the broadening at half the maximum intensity (Full Width Half Maximum, FWHM) in radians, and k is a shape factor, typically valued at 0.89. The scattering vector q is defined as $q = \frac{4\pi Sin\theta}{\lambda}$, and the broadening of q at half the maximum intensity is referred to as Δq. Applying a Lorentzian curve to the first strong peak of different phases within their SAXS pattern results in the determination of the peak position, represented as q, along with the corresponding Δq value associated with that phase. Furthermore, the correlation length is typically scaled relative to the lattice parameter, thereby providing a measure of the spatial length scale of correlation in relation to the dimensions of the molecular length scale.

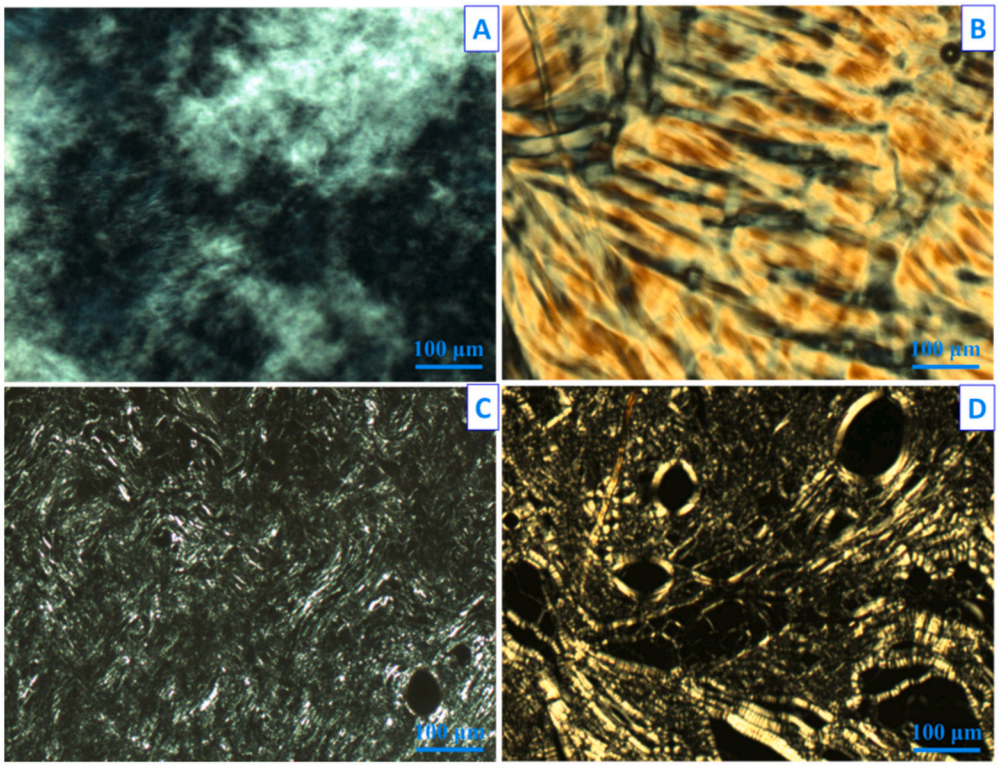

Fig. 2. Polarizing optical microscopy (POM) textures of (A) H phase at $\alpha = 0.0$, $\Phi_s = 50$ & $T = 40\,^{\circ}C$, (B) H phase at $\alpha = 0.1$, $\Phi_s = 50$ & $T = 40\,^{\circ}C$, (C) L_α phase at $\alpha = 0.2$, $\Phi_s = 50$ & $T = 40\,^{\circ}C$ and (D) L_α phase at $\alpha = 0.3$, $\Phi_s = 50$ & $T = 40\,^{\circ}C$, in the SDS-PTHC-water system. H and L_α denote the hexagonal and lamellar phases, respectively. The L_α phase found to be coexist with excess water which show black region under POM.

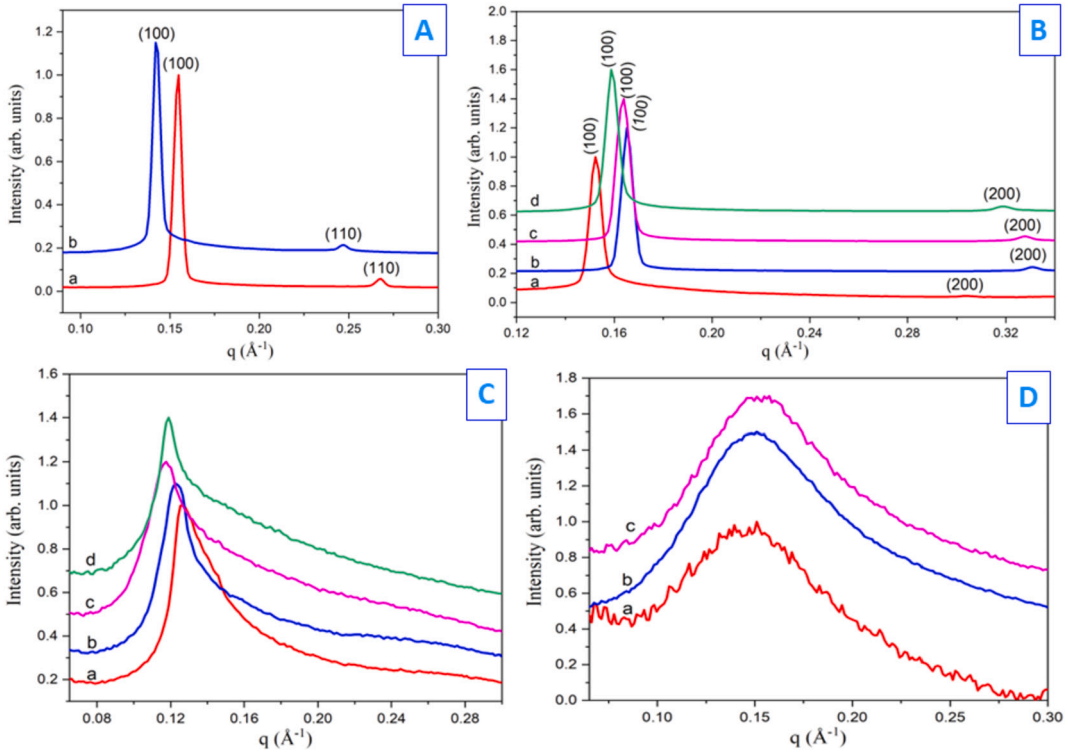

Fig. 3. X-ray diffraction pattern of the SDS-PTHC-water system. (A) exhibiting H phase at $\Phi_s = 50$, $T = 40\,^{\circ}C$ and: (a) $\alpha = 0.0$ curve in red color, (b) $\alpha = 0.1$ curve in blue color. (B) showing L_α phase at $\Phi_s = 50$, $T = 40\,^{\circ}C$ and: (a) $\alpha = 0.2$ curve in red color, (b) $\alpha = 0.3$ curve in blue color, (c) $\alpha = 0.4$ curve in pink color, (d) $\alpha = 0.5$ curve in green color. The L_α phase is found to be coexist with excess water. (C) exhibiting $L_\alpha + L_x$ phase at $\Phi_s = 50$, $T = 40\,^{\circ}C$ and: (a) $\alpha = 0.7$ curve in red color, (b) $\alpha = 0.8$ curve in blue color, (c) $\alpha = 0.9$ curve in pink color and (d) $\alpha = 1.0$ curve in green color. (D) showing L_x phase at $\Phi_s = 50$, $T = 40\,^{\circ}C$ and: (a) $\alpha = 1.1$ curve in red color, (b) $\alpha = 1.2$ curve in blue color and (c) $\alpha = 1.3$ curve in pink color. The $L_\alpha + L_x$ and L_x phases are found to be coexist with excess water.

Table 2
Variation of correlation length, ξ and no. of correlated units (ξ/lp) in the various phases observed in SDS-PTHC-water system at $\Phi_s = 50$ and T = 40 °C. lp is the lattice parameter which is equivalent to the parameter a in the H phase and the value d in the L_α phase.

α	Lattice Parameter (Å)	Correlation length ξ(Å)	ξ/lp (approx.)	Phase
0.0	47.25	1436.8	30	H
0.1	51.11	1350.0	26	H
0.2	41.26	1052.6	25	$I + L_\alpha$
0.3	38.06	1312.0	34	$I + L_\alpha$
0.4	38.32	1279.0	33	$I + L_\alpha$
0.5	39.58	1189.0	30	$I + L_\alpha$
0.6	43.45	780.6	18	$I + L_\alpha$
0.7-1.0	–	–	–	$I + L_\alpha + L_x$
1.1	41.58	64.0	2	$I + L_x$
1.2	41.47	68.9	2	$I + L_x$
1.3	41.72	86.0	2	$I + L_x$

This results in a dimensionless value, denoted as $\frac{\xi}{lattice\ parameter}$ that is ($\frac{\xi}{lp}$, lp is the lattice parameter), which is essential for facilitating comparison.

The variation in the correlation length, denoted by ξ, relative to the lattice parameter of the phase, across the different phases of the SDS-PTHC-water system as α increases from 0.0 to 1.3 and at $\Phi_s = 50$ & $T = 40\,°C$, is detailed in the table [Table 2]. It is observed that in the H phase, the correlation length is approximately 1400 Å, leading to the formation of around 30 correlated cylindrical micelle units within the cylindrical plane. Additionally, in the $I + L_\alpha$ phase, the correlation length is found to be slightly shorter at about 1200 Å, indicating the presence of approximately 30 correlated bilayers along the normal to the bilayer surface. Nonetheless, it has been noted that the correlation length within the $I + L_x$ phase is significantly reduced to around 70 Å, corresponding to about 2 correlated bilayer units. This suggests a short-range positional order within this phase. Moreover, the substantial number of associated units observed in both the H and $I + L_\alpha$ phases (L_α phase with excess water) confirms a long-range positional order within these phases. For a deeper understanding of the electronic distribution within the H and L_α phases, an electron density map associated with these phases has been further reconstructed by using procedures as described by S. P. Gupta et al. [26]; the details of this reconstruction can be found below.

By employing the method of inverse Fourier transformation, the scattering amplitude, denoted by $F_s(hkl)$, of a liquid-crystalline (mesophase) phase is linked to its electron density profile, represented by $\rho(x, y, z)$ as;

$$\rho(x, y, z) = \sum_{hkl} F_s(hkl) e^{2\pi i(hx+ky+lz)} \tag{1}$$

In the given formula, (hkl) represents the Miller indices of the planes corresponding various reflected peaks observed in SAXS pattern's of the phases, while x, y, and z denote the fractional coordinates within the unit cell. The scattering amplitude, denoted by $F_s(hkl)$, is a complex quantity. It can be expressed as the product of its phase, $\Phi(hkl)$, and its magnitude, which is denoted as $|F_s(hkl)|$. The magnitude $|F_s(hkl)|$ exhibits a direct proportionality to the square root of the intensity, $I(hkl)$, of the reflected X-ray radiation. Thus;

$$F_s(hkl) = |F_s(hkl)| e^{\Phi(hkl)} = \sqrt{I(hkl)} e^{\Phi(hkl)} \tag{2}$$

To ascertain the intensities of the distinct peaks observed in various phases in their SAXS pattern, one proceeds by computing the area beneath each peak following the subtraction of the background, and applying the requisite geometric and multiplicity adjustments. For each diffraction peak, the phase variable $\Phi(hkl)$ stands alone as the information that cannot be directly retrieved from the SAXS experiment. However, when the structure under investigation is centrosymmetric, this issue becomes amenable to solution, indicating that $\Phi(hkl)$ may only assume values of 0 or π. This is justified by the fact that scattering amplitude, $F_s(hkl)$, can only be real if the electron density distribution profile is centro-symmetric (i.e., $\rho(-x, -y, -z) = \rho(x, y, z)$. Consequently, any phase value ranging from 0 to 2π can represent the phase for non-centro-symmetric groups. Given that the phases H and L_α that have been observed are centro-symmetric, the process of reconstructing electron density maps becomes a straightforward endeavor. This involves interpreting the phase variable $\Phi(hkl)$ as either 0 or π. Subsequently, the most appropriate map is determined based on the quality of the reconstructed electron density maps, alongside additional physical and chemical data pertaining to the system, such as the size and composition of the constituent chemical species.

Fig. 4(A,B) presents the reconstructed electron density maps for the H phase, which were observed at $\alpha = 0.0$ and 0.1, $\Phi_s = 50$, and $T = 40\,°C$. These reconstructions are derived from the pertinent information derived from the Miller indexing of the peak, including its intensity, multiplicity, and phase as outlined in table [Table 1]. Highlighted in deep pink are the regions of highest electron density, while those represented in deep green denote the regions of lowest electron density. The depicted maps illustrate a 2D hexagonal lattice arrangement, as observed in regions of low electron density, which align with the alkyl chain of the surfactant, SDS.

The discussion previously covered the SDS-PTHC-water system at various molar ratios ($\alpha = 0.2$, $\alpha = 0.3$, $\alpha = 0.4$, $\alpha = 0.5$) and $\Phi_s = 50$ & $T = 40\,°C$, the L_α phase is found to be stabilized along with the excess water. The reconstructed electron density maps for the L_α phase at these compositions have been provided in the figure [Fig. 4(C, D) & supporting Figure S5], along with related parameters such as peak intensity, Miller indices, multiplicity, and phase of the peak, as detailed in the accompanying table [Table 1]. The maps display a stripe-like pattern, characterizing the distribution of water and bilayer regions, respectively, with the former represented by areas of high electron density and the latter by areas of low electron density. Therefore, low electron density bilayers become apparent as a one-dimensional periodic lamellar structure within the context of a high electron density water matrix.

A thorough analysis of the SAXS data pertaining to the L_α phase is undertaken through the application of a methodology crafted by Pabst et al. [23]. It is important to note that the L_α phase can be understood either through the convolution of the bilayer electron density profile by a series of parallel planes, each spanned by a distance corresponding to the lamellar periodicity, or through the convolution of a bilayer by a set of one-dimensional lattice points, also separated by distances matching the lamellar periodicity [Fig. 5]. It is the former interpretation that Pabst et al. opt for, aiming to formulate a theory that elucidates the scattered intensity profile, which results from the interaction between the L_α phase and X-rays of wavelength λ, alongside the scattering wavevector $q = \frac{4\pi\ Sin(\theta)}{\lambda}$, where 2θ is the scattering angle.

The Fourier transform of the electron density profile across the bilayer is referred to as the form factor amplitude, denoted by $f(q)$, while its squared value is directly proportional to this amplitude, termed the form factor, $F(q)$. Similarly, the Fourier transform of the array of parallel planes, referred to as the structure factor amplitude, $s(q)$, and its squared value, known as the structure factor, $S(q)$, exhibits a proportional relationship. Furthermore, the scattered intensity, $I(q)$, resulting from the phase is directly proportional to the product of the form factor, $F(q)$, and the structure factor, $S(q)$. The equation for the scattered intensity, $I(q)$, from the L_α phase is expressed as:

$$I(q) = scale[\frac{(1 - N_d)S(q)|f(q)|^2}{q} + \frac{N_d|f(q)|^2}{q}] \tag{3}$$

The entire expression is subject to division by q, which represents the denominator of the aforementioned equation, because of the geometric considerations used in present SAXS experiments. This factor is intricately linked to both the geometry of the detection device employed for data collection and the nature of the sample being analyzed. The partic-

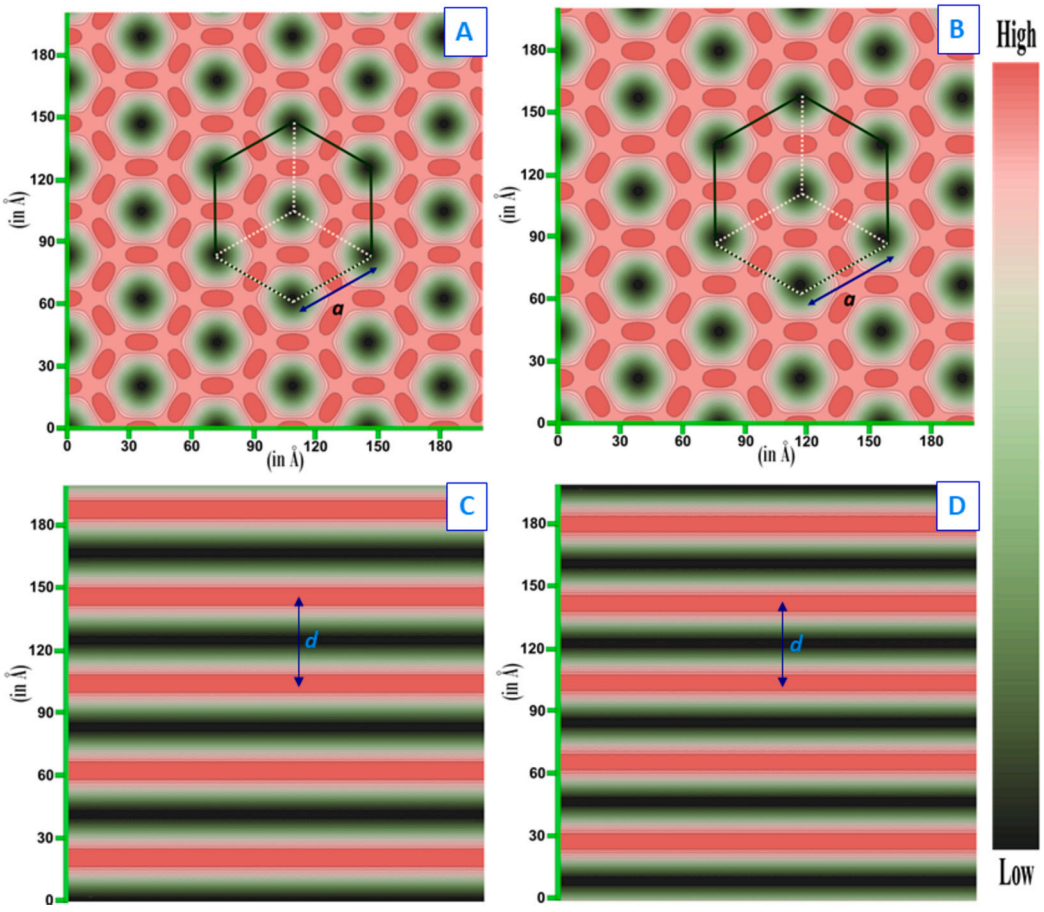

Fig. 4. Reconstructed electron density maps of the SDS-PTHC-water system at: (A) $\alpha = 0.0$, $\Phi_s = 50$ & $T = 40\,^{\circ}C$ corresponding to the H, (B) $\alpha = 0.1$, $\Phi_s = 50$ & $T = 40\,^{\circ}C$ corresponding to the H. Hexagon shows the conventional unit cell of the 2D hexagonal lattice and there are three primitive unit cells within this conventional unit cell. a is the lattice parameter. (C) $\alpha = 0.2$, $\Phi_s = 50$ & $T = 40\,^{\circ}C$ corresponding to the L_α phase and (D) $\alpha = 0.3$, $\Phi_s = 50$ & $T = 40\,^{\circ}C$ corresponding to the L_α phase. d is the lamellar periodicity. Deep pink represents the highest electron density and deep green is the lowest.

ular shape of the detector, described as being two-dimensional, and the captured SAXS patterns of the L_α phase (as well as L_x phase), which are unoriented, result in the determination of the geometric factor being equivalent to q. The $S(q)$ symbolizes the structure factor associated with a sequence of parallel planes, while $f(q)$ denotes the amplitude of the form factor of the bilayer profile. The final component of equation [Equation (3)] pertains to diffuse scattering, a phenomenon that is often neglected when structural information is solely derived from Bragg peaks. In this context, N_d represents the fraction of diffuse scattering.

The form factor amplitude, $f(q)$ is derived from the Fourier transform of the electron density profile, denoted as $\rho(z)$, across the bilayer. In this context, z denotes the axis that is perpendicular to the bilayer plane and the profile, $\rho(z)$ is characterized by three Gaussian functions, each encapsulating distinct regions of the molecule. The two Gaussian functions, which are symmetrically situated with respect to the bilayer center and correspond to the head-groups of SDS molecules, are described by a Full width at half maxima (FWHM), σ_h, situated at a distance $z = \pm z_h$ from the center. The third Gaussian function, which corresponds to the terminal methyl groups, is defined by a FWHM σ_c at the center of the bilayer ($z = 0$).

$$\rho(z) = \rho_{CH_2} + \rho_h\,[exp(-\frac{(z-z_h)^2}{2{\sigma_h}^2}) + exp(-\frac{(z+z_h)^2}{2{\sigma_h}^2})] + \rho_c\,[exp(-\frac{z^2}{2{\sigma_c}^2})] \tag{4}$$

In this context, the electron densities of both the head group, denoted as ρ_h, and the hydrocarbon tail, represented by ρ_c, are determined in relation to the methylene electron density, symbolized by ρ_{CH_2}. This framework results in the formulation of the form factor amplitude as outlined below.

$$f(q) = 2\sqrt{2\pi}\,\sigma_h\,\rho_h[exp(-\frac{{\sigma_h}^2 q^2}{2})]\,cos(qz_h) + \sqrt{2\pi}\,\sigma c\,\rho_c\,[exp(-\frac{{\sigma_c}^2 q^2}{2})] \tag{5}$$

Moreover, pursuant to the modified Caille theory, the structure factor, $S(q)$ is defined as follows:

$$S(q) = N + 2\sum_{k=1}^{N-1}(N-k)cos(qkd) \times e^{-(d/2\pi)^2 q^2 \eta\gamma}\,\pi k^{-(d/2\pi)^2 q^2 \eta} \tag{6}$$

In the context of this model, N denotes the mean number of coherent (correlated) scattering bilayers present within the stack. The constant γ signifies Euler's constant, while d represents the lamellar periodicity. Furthermore, the Caille's parameter, denoted by $\eta = (q^2 k_B\,B\,T)/(8\pi\sqrt{K\,B})$, encompasses the following variables: K and B, which correspond to the bending and bulk moduli, respectively, of the lamellar stack, k_B is the Boltzmann constant. Model parameters such as σ_h, σ_c, ρ_h, ρ_c, z_h, η, in conjunction with N and N_d, are fine-tuned to achieve the optimal alignment between the observed and calculated intensity profiles.

The SAXS pattern of the L_α phase, occurring at $\alpha = 0.3$, $\Phi_s = 50$, and temperature $T = 40\,^{\circ}C$, is exquisitely represented by this model. The data is represented by a half filled deep cyan diamond, with the curve fitting it marked in red [Fig. 6A]. The electron density profile derived from the model is depicted in red in the inset of the figure [Fig. 6A (inset)], and the relevant model parameters are elaborated in table [Table 3].

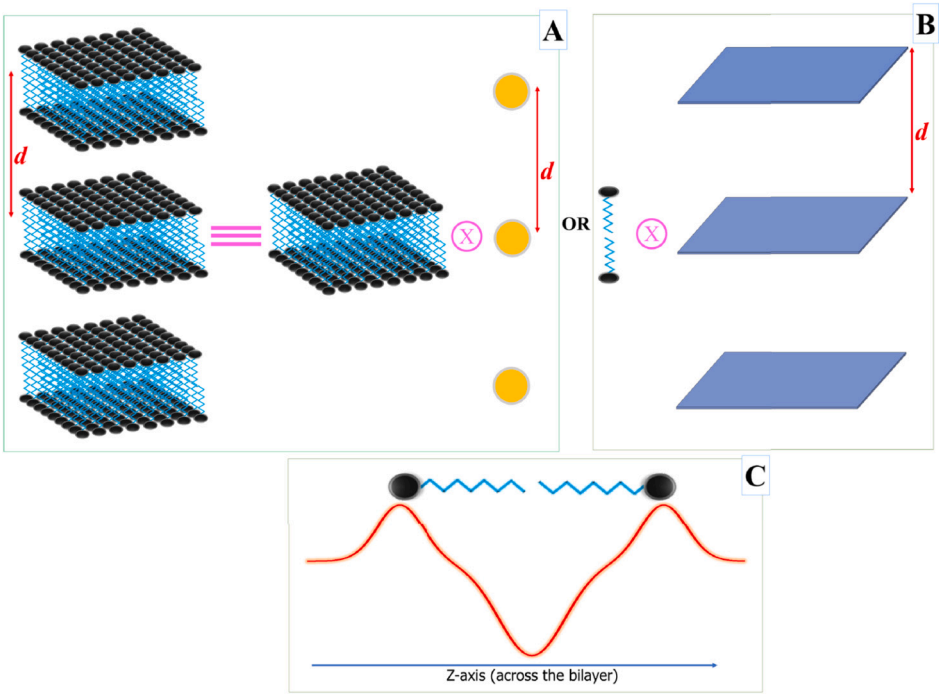

Fig. 5. (A) The lamellar (L_α) phase which is the set of bilayers separated by water can be considered as the convolution of bilayer with the set of imaginary points (circles in bright yellow color) separated by a distance equal to the lamellar periodicity (d) or (B) can be also considered as the convolution of the bilayer electron density profile across the bilayer with the set of parallel planes (plane in deep blue color) separated by a distance equal to the lamellar periodicity. (C) Bilayer electron density profile across the bilayer can be model as the combination of three Gaussians (curve in orange color); The two Gaussian functions, which are symmetrically situated with respect to the bilayer center and correspond to the head-groups of SDS molecules, the third Gaussian function, which corresponds to the terminal methyl groups, at the center of the bilayer.

The electron profile across the bilayer is represented in relation to the CH_2 group electron density, which is arbitrarily designated as zero and depicted as a black, dotted line. The corresponding calculated form factor ($F(q) = f(q)^2$) variation is illustrated using a half-filled diamond symbol with black coloration and structure factor ($S(q)$) is depicted in such a diamond symbol with red coloration as represented in figure [Fig. 6B]. The structure factor exhibits two distinct, highly correlated peaks, whereas the form factor experiences more gradual variation. It should be noted that the theoretical intensity is directly related to the product of the form factor and structure factor.

The SAXS data from the L_x phase was attempted to be aligned with the predicted scattering patterns from the sponge phase, as outlined in the reference [27]. However, it proved to be challenging to identify a suitable combination of model parameters that would yield a satisfactory fit. Furthermore, the mesh size in the sponge phase, defined by the position of the broad peak, typically corresponds to 1.5 times the lamellar periodicity of the L_α phase at a given water content. Conversely, the average spacing of the L_x phase is found to be comparable to the L_α phase periodicity. These discrepancies lead us to dismiss the hypothesis that the L_x phase represents a conventional sponge phase.

The L_x phase may encompass bilayer-like aggregates, as inferred from the observation of flow-birefringence within this phase and the parallel similarity in average spacing to that of the L_α phase periodicity. The manifestation of a broad peak within this phase, in contrast to that observed in the L_α phase, may result from the irregular stacking of these aggregates. Given that the number of correlated bilayers (N) in the model for the L_α phase is a variable parameter, it can also serve to elucidate the irregular stacking of bilayers. Therefore, we have delineated the SAXS data corresponding to the L_x phase, utilizing the aforementioned model. It is imperative to note that within the L_x phase, the parameter denoted by η, the Caille parameter, is merely a fitting parameter devoid of the physical significance it attains in the L_α phase

This model aligns particularly well with the SAXS pattern observed for the L_x phase observed at $\alpha = 1.3$, $\Phi_s = 50$, and $T = 40\,^\circ$C, as depicted in figure [Fig. 6C] where data is shown by half filled diamond in deep cyan color along with fit in pink color. The accompanying table, labeled as [Table 3], outlines the corresponding model parameters, while figure [Fig. 6C (inset)] illustrates the electron density profiles inferred from the analysis. The corresponding calculated form factor, represented by $F(q) or (f(q)^2)$, is depicted in a half-filled diamond with a black color and structure factor ($S(q)$) is shown in such a half-filled diamond symbol with a red color, as display in figure [Fig. 6D]. Conversely, the structure factor, along with the form factor, displays a broad and smooth variation with respect to the wave vector. Despite the L_α phase being associated with thirty correlated bilayers, the L_x phase exhibits only two distinct correlated bilayers.

To conduct a comparative analysis of the theoretical electron density variations across the bilayer in both the L_α and L_x phases, we have plotted the electron density profiles of the two phases together, shown in the figure [Fig. 7]. As observed, there is a gradual and nuanced alteration in the electron density profile during this transition from the L_α to L_x phase. This suggests that the L_x phase can be characterized by a disordered arrangement of bilayers, exhibiting short-range positional correlations.

Moreover, the thickness of the bilayer, denoted as d_B, is determined through the equation $d_B = 2\ z_h + \sigma_h$, as described in the framework given by Pabst et al. [23]. By applying this relation to the L_α and L_x phases, it was found that the bilayer thickness is approximately 32.14 Å and 35.82 Å, respectively, in these phases. Consequently, this yields an approximate size for the SDS molecule, ranging from 16.07 Å in the L_α phase to 17.91 Å in the L_x phase. Nonetheless, the SDS micelles present challenges in accurately determining their size within a solution. However, both experimental evidence and theoretical calculations suggest that the radius of these micelle spheres ranges from approximately 16Å to 21Å [28], our derived value is in agreement with both theoretical and experimental determinations.

The phase behavior of the current system can be succinctly described as follows: At a specific value of $\Phi_s = 50$ and $T = 40\,^\circ$C, it transitions

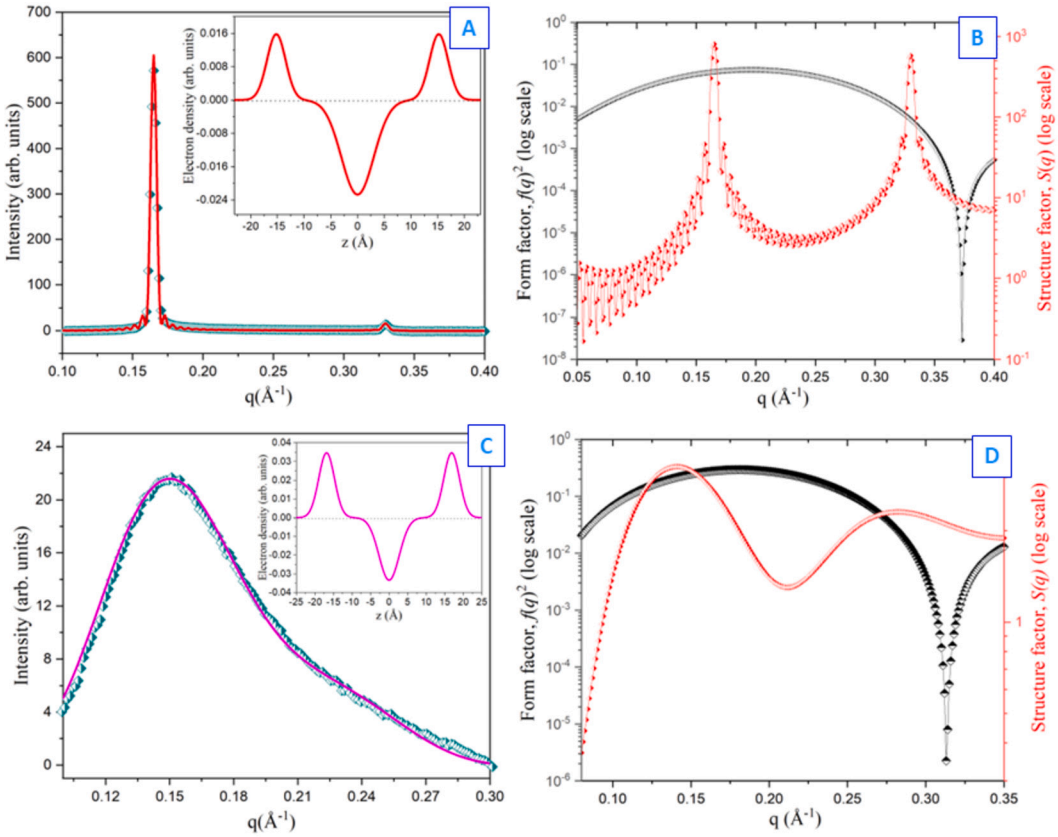

Fig. 6. (A) Small angle X-ray scattering data of the L_α phase shown as half-filled diamond in deep cyan color along with fit curve in red color and the derived electron density profile across the bilayer is shown in the red color in inset and (B) Showing the variation of the corresponding form factor ($F(q) = f(q)^2$), illustrated using a half-filled diamond symbol with black coloration and structure ($S(q)$) is depicted in such a diamond symbol with red coloration, (C) Small angle X-ray scattering data of the L_x phase shown as half-filled diamond in deep cyan color along with fit curve in pink color and the derived electron density profile across the bilayer is shown in the pink color in inset and (D) Showing the variation of the corresponding form factor ($F(q) = f(q)^2$), illustrated using a half-filled diamond symbol with black coloration and structure ($S(q)$) is depicted in such a diamond symbol with red coloration.

Table 3
Values of parameters obtained from the fit of the small angle X-ray scattering data at $\Phi_s = 50$ and $T = 40\,°C$ of the SDS-PTHC-water system to the model of lamellar phase as described by Pabst et al. using three Gaussian profile of the bilayer.

α	σ_h(Å)	σ_c(Å)	$(\rho_c)/(\rho_h)$	z_h(Å)	η	N	N_d	d(Å)	Phase
0.3	1.74	3.02	-1.44	15.20	0.031	30	0	38.06	$I + L_\alpha$
1.3	2.12	2.73	-0.97	16.85	0.278	2	0.4	41.72	$I + L_x$

through a sequence of phases: $H \rightarrow I + L_\alpha \rightarrow I + L_x$, with an increase in concentration of PTHC. As a hydrotrope, PTHC exhibits a tendency to aggregate near the interface between water and oil, altering its interface curvature. The addition of PTHC modifies the morphology of the cylindrical micelles formed by SDS at $\Phi_s = 50$ and $T = 40\,°C$, resulting in a reduction in their curvature. This leads to the formation of worm-like micelles that retain the H phase and are organized in a 2D hexagonal lattice structure. Nonetheless, the L_α phase gains prominence once PTHC is introduced beyond a certain threshold, attributed to a notable reduction in micelle curvature. The addition of more PTHC further disrupts the long-range organization of L_α and solidifies the L_x phase of short range positional order.

Hydrotropes are closely related to the modulation of critical micelle concentration and the morphology of micelle formation within surfactant self-assembly [22,29–31]. For instance, p-toluidine halides have been observed to significantly alter the viscoelasticity properties of anionic surfactant solutions, which in turn is directly linked to changes in the morphology of the surfactant solution. In this regard, S. K. Ghosh et al. have documented the addition of PTHC to SDS at a fixed Φ_s of 40, which resulted in a transition from a hexagonal to a lamellar structure of the surfactant solution, as the ratio of PTHC to SDS (α) varied. This transition was observed through a nematic phase of rodlike micelles (N_C) to isotropic (I) to a nematic phase of disklike micelles (N_D) [22,31]. This study suggests that the morphology of surfactant micelles can be easily adjusted by hydrotropes, thereby modifying the phase behavior and rheological properties of concentrated surfactant solutions.

S. P. Gupta et al. have conducted research on the impact of SHN, a hydrotropes, on the phase behavior of cetylpyridinium chloride (CPC), a compound recognized for its antiseptic and antimicrobial properties, widely utilized in numerous over-the-counter products, including mouthwashes, toothpastes, lozenges, throat sprays, breath sprays, nasal sprays, and pre-moistened wipes. The study revealed that the mixture of CPC-SHN-water displays a variety of intermediate phases, including ribbon, cubic, random mesh, hexagonal ordered mesh, tetragonal ordered mesh, and nematic phase of rodlike micelles, as well as hexagonal, lamellar phases [9]. Furthermore, it was observed that an increase in SHN concentration led to the emergence of an isotropic phase of bilayer, which bears a striking resemblance to the 'L_x' phase [32].

It has been established that the inter-lamellar correlations diminish to the short-range as the quasi-long-range positional arrangement of

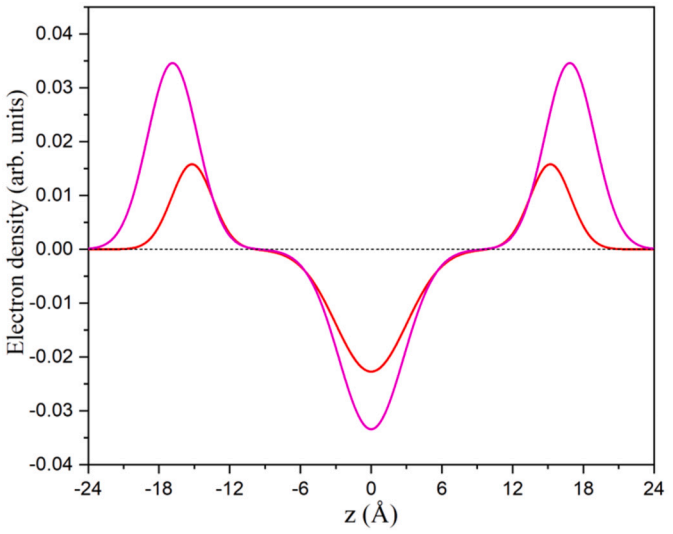

Fig. 7. Demonstrating the variation in electron density profile across the bilayer as derived from the model, the curve represents the L_α phase, depicted in red, and the L_x phase, illustrated in pink. The electron density is depicted in relation to the electron density of the CH_2 group, which has been arbitrarily assigned a value of zero and represented as a black, dotted line. z referred to the axis normal to the bilayer plane.

the L_α phase is compromised by a particular density of unbound dislocations. The influence of dislocation loops on the L_α phase has been explored within the context of the smectic A - nematic liquid crystal transition, as theorized in the references [33,34]. In such scenarios, dislocation loops within a bilayer stack correspond to the pores or channels may be observed in the bilayer.

In the context of the current study, it is anticipated that electrostatic interactions will be diminished at elevated concentrations of salt (PTHC), thereby modifying the Gaussian curvature of the bilayer. This modification is expected to confer a weakly negative Gaussian curvature on the resulting structure, thereby enhancing the stability of the pores, as has been observed in various systems capable of sponge formation, such as listed in the reference [35]. Moreover, the formation of pores and channels is also projected in this scenario.

The primary distinction that will be observed between the system under investigation and those that lead to the formation of a L_3 phase, is attributed to the nature of inter-bilayer interactions. The system currently under consideration is anticipated to undergo a phase characterized by moderate swelling, owing to the attractive van der Waals interactions. In contrast, systems experiencing significant swelling due to steric repulsion are expected to exhibit a phase characterized by sponge formation.

It is noteworthy that a ternary system comprising water, anionic surfactants with calcium or magnesium ions, and branching co-surfactants presents an additional variant of the L_3 phase, as documented in the references [36,37]. A distinguishing characteristic of this phase is the observation of a broad correlation peak in its X-ray diffraction pattern, which is found to be positioned near the location of a more pronounced peak observed in the L_α phase. Nonetheless, in the context of the L_3 phase delineated in the preceding scholarly works, it is observed that the d-spacing indicative of broad correlation peaks is approximately equivalent to 1.5 times the lamellar periodicity of the L_α phase, this suggests a high degree of similarity between this variant of the L_3 phase and the present L_x phase.

It is frequently noted that the L_3 phase emerges when the physicochemical parameters of the system are modified to enhance the lipophilicity of the dilute L_α phase. In the case of non-ionic surfactants, increasing their lipophilicity can be achieved by elevating the temperature or adjusting the ratio of the cosurfactant to the surfactant concentration, as outlined in [38,39]. Nonetheless, the elevation of lipophilicity in the L_α phase has been demonstrated to inhibit the formation of the L_3 phase under certain other conditions, as reported in the reference [40]. Conversely, the presence of the L_3 phase is notably absent with alcohols of perfluorinated chain lengths or in those with longer chain lengths, but it is commonly observed in zwitterionic surfactants featuring intermediate-chain alcohols, as detailed in [41]. Within the framework of the structure of the L_3 phase, researchers Cates et al. undertook an independent theoretical investigation, while Porte et al. initiated the first experimental analysis. Both groups suggested that the molecules of both surfactants and cosurfactants present in the L_3 phase aggregate to form a continuous network structure, as evidenced by their respective findings in the references [42,43].

Furthermore, the L_3 phase is observed in the systems comprising the bilayer-forming surfactant, dodecyldimethylammonium bromide (DDAB), and the ionic polymer salt, polyelectrolyte sodium polyacrylate (PAANa), in conjunction with the collapsed lamellar (L_α) phase. It is noted that both low and high salt concentrations result in lamellar structures exhibiting reduced periodicities, which are secured by the presence of polymer bridging, and held together by van der Waals attraction, respectively [44]. The sponge phase, characterized by the swelling complex at intermediate salt concentrations, suggests that the modification of the bilayer's elastic moduli is a consequence of the polymer adsorption process.

In the current system, a highly concentrated salt solution is capable of dissolving a moderately concentrated phase labeled as L_α, leading to the emergence of the L_x phase. Nonetheless, it has been observed that co-surfactants, such as alcohols, are not indispensable for stabilizing the L_x phase. This observation implies that a sufficient concentration of organic salt alone is sufficient to neutralize the charges carried by the ionic surfactant, thereby facilitating the formation of the L_x phase, which is characterized by short-range attractive forces. As previously stated, the L_x phase exhibits optical isotropic properties and potentially incorporates a structure of pores that may function as drug delivery systems for therapeutically active substances.

4. Conclusion

In conclusion, the impact of PTHC, an organic salt, on the phase behavior of SDS, an anionic surfactant, has been meticulously investigated. Through the application of POM and SAXS techniques, we have conducted an analysis of the SDS-PTHC-water system operating at $T = 40\,^{\circ}\mathrm{C}$, $\Phi_s = 50$ and various values of α. An analysis reveals that as the concentration of PTHC increases, the system shows distinct phases corresponding to H, $I + L_\alpha$, and $I + L_x$ phases. For both H and L_α phases, electron density maps have been precisely reconstructed. The L_α and L_x phases have been comprehensively explained by the model of lamellar phase, indicating that the L_x phase is characterized by bilayer structures, thereby facilitating short range positional correlation. This research underscores the potential for stabilizing the L_x phase by effectively neutralizing the charges of the ionic surfactant with high concentrations of organic salt.

CRediT authorship contribution statement

Mukesh Chandra Bos: Writing – original draft, Data curation, Conceptualization. **Shallu Dhingra:** Writing – original draft, Data curation, Conceptualization. **Manoj Kumar Srivastava:** Data curation, Conceptualization. **Pawan Kumar:** Data curation, Conceptualization. **Divesh Kumar:** Data curation, Conceptualization. **Santanu Kumar Pal:** Writing – review & editing, Visualization, Funding acquisition, Data curation, Conceptualization. **Santosh Prasad Gupta:** Writing – review & editing, Writing – original draft, Visualization, Funding acquisition, Data curation, Conceptualization.

Declaration of competing interest

The author declares that this article does not have a potential conflict of interest. This article also does not contain any studies with human or animal subjects.

Acknowledgements

S. P. Gupta acknowledges the Patna University for its technical support. S. P. Gupta expresses gratitude to SERB-TARE (TAR/2021/000146) for fellowship and for the financial support. S. K. Pal thanks SERB-TARE (TAR/2021/000146) for the financial support.

Appendix A. Supplementary material

Supplementary material related to this article can be found online at https://doi.org/10.1016/j.molliq.2024.126485.

Data availability

The authors confirm that the data supporting the findings of this study are available within the article and/or its supplementary materials.

References

[1] J. Israelachvili, Intermolecular and Surface Forces, 2nd ed., Academic Press, London, 1991.
[2] P. Sar, A. Ghosh, A. Scarso, B. Saha, Surfactant for better tomorrow: applied aspect of surfactant aggregates from laboratory to industry, Res. Chem. Intermed. 45 (2019) 6021–6041, https://doi.org/10.1007/s11164-019-04017-6.
[3] O. Massarweh, A.S. Abushaikha, The use of surfactants in enhanced oil recovery: a review of recent advances, Energy Rep. 6 (2020) 3150–3178, https://doi.org/10.1016/j.egyr.2020.11.009.
[4] R.G. Laughlin, The Aqueous Phase Behavior of Surfactants, Academic Press, London, 1994.
[5] T.F. Tadros, Self-Organized Surfactant Structures, 1st ed., Wiley-VCH, Germany, 2011.
[6] N.A. Falk, Surfactants as antimicrobials: a brief overview of microbial interfacial chemistry and surfactant antimicrobial activity, J. Surfactants Deterg. 22 (2019) 1119–1127, https://doi.org/10.1002/jsde.12293.
[7] J.M. Seddon, R.H. Templer, in: R. Lipowsky, E. Sackmann (Eds.), Handbook of Biologicalphysics, Elsevier, Amsterdam, 1995.
[8] William M. Gelbart, Avinoam Ben-Shaul, Didier Roux (Eds.), Micelles, Membranes, Microemulsions, and Monolayers, Springer, 1994.
[9] S.P. Gupta, V.A. Raghunathan, Controlling the thermodynamic stability of intermediate phases in a cationic-amphiphile–water system with strongly binding counterions, Phys. Rev. E 88 (2013) 012503, https://doi.org/10.1103/PhysRevE.88.012503.
[10] E. Kaler, A.K. Murthy, B.E. Rodriguez, J.A.N. Zasadzinski, Spontaneous vesicle formation in aqueous mixtures of single-tailed surfactants, Science 245 (4924) (1989) 1371–1374, https://doi.org/10.1126/science.2781283.
[11] S.P. Gupta, Investigation of ordered mesh phases using their detailed reconstructed electron density maps, J. Mol. Liq. 315 (2020) 113831, https://doi.org/10.1016/j.molliq.2020.113831.
[12] P.A. Hassan, S.R. Raghavan, E.W. Kaler, Microstructural changes in sds micelles induced by hydrotropic salt, Langmuir 18 (7) (2002) 2543–2548, https://doi.org/10.1021/la011435i.
[13] S.K. Ghosh, R. Ganapathy, R. Krishnaswamy, J. Bellare, V.A. Raghunathan, A.K. Sood, Structure of mesh phases in a cationic surfactant system with strongly bound counterions, Langmuir 23 (2007) 3606–3614, https://doi.org/10.1021/la0631466.
[14] W. Helfrich, Z. Naturforsch. A 33 (1978) 305.
[15] D. Roux, C. Coulon, M.E. Cates, Sponge phases in surfactant solutions, J. Phys. Chem. 96 (11) (1992) 4174–4187, https://doi.org/10.1021/j100190a017.
[16] G. Porte, J. Appell, P.B. et, J. Marignan, L to l3: a topology driven transition in phases of infinite fluid membranes, J. Phys. France 50 (1989) 1335–1347, https://doi.org/10.1051/jphys:0198900500110133500.
[17] D. Gazeau, A.M. Bellocq, D. Roux, T. Zemb, Experimental evidence for random surface structures in dilute surfactant solutions, Europhys. Lett. 9 (5) (1989) 447, https://doi.org/10.1209/0295-5075/9/5/007.
[18] X-ray and neutron-scattering study of the lamellar and l3 phases of the system aerosol-ot-water.
[19] A. Pal, G. Pabst, V.A. Raghunathan, Defect-mediated lamellar-isotropic transition of amphiphile bilayers, Soft Matter 8 (2012) 9069–9072, https://doi.org/10.1039/C2SM26535D.
[20] A. Pal, P. Bharath, S.G. Dastidar, V.A. Raghunathan, Collapse and coacervation of a lamellar phase by inter-headgroup bridging, Soft Matter 8 (2012) 927–930, https://doi.org/10.1039/C2SM06817F.
[21] P. Kékicheff, B. Cabane, Between cylinders and bilayers: structures of intermediate mesophases of the sds/water system, J. Phys. 48 (9) (1987) 1571–1583, https://doi.org/10.1051/jphys:019870048090157100ff.
[22] S.K. Gosh, Influence of strongly bound counterions on the phase behaviour of ionic amphiphiles, Thesis, 2007.
[23] G. Pabst, M. Rappolt, H. Amenitsch, P. Laggner, Structural information from multilamellar liposomes at full hydration: full q-range fitting with high quality x-ray data, Phys. Rev. E 62 (2000) 4000, https://doi.org/10.1103/PhysRevE.62.4000.
[24] D. Constantin, P. Oswald, M. Impéror-Clerc, P. Davidson, P. Sotta, Connectivity of the hexagonal, cubic, and isotropic phases of the c12eo6/h2o lyotropic mixture investigated by tracer diffusion and x-ray scattering, J. Phys. Chem. B 105 (3) (2001) 668–673, https://doi.org/10.1021/jp002672h.
[25] P. Oswald, J. Géminard, L. Lejcek, L. Sallen, Nonlinear analysis of stripe textures in hexagonal lyotropic mesophases, J. Phys. II France 6 (1996) 281–303, https://doi.org/10.1051/jp2:1996182.
[26] S.P. Gupta, M. Gupta, S.K. Pal, Highly resolved morphology of room-temperature columnar liquid crystals derived from triphenylene and multialkynylbenzene using reconstructed electron density maps, ChemistrySelect 2 (21) (2017) 6070–6077, https://doi.org/10.1002/slct.201701117.
[27] L. Porcar, W.A. Hamilton, P.D. Butler, G.G. Warr, Scaling of structural and rheological response of l3 sponge phases in the sweetened cetylpyridinium/hexanol/dextrose/brine system, Langmuir 19 (26) (2003) 10779–10794, https://doi.org/10.1021/la034661w.
[28] G. Duplâtre, M.F.F. Marques, M. da Graça Miguel, Size of sodium dodecyl sulfate micelles in aqueous solutions as studied by positron annihilation lifetime spectroscopy, J. Phys. Chem. 100 (41) (1996) 16608–16612, https://doi.org/10.1021/jp960644m.
[29] M.S. Sheikh, A.J. Khanam, N. Shafi, A. Amin, M.A. Rub, Effect of hydrotropes on the micellization behavior of sodium dodecyl sulfate/sodium dodecyl benzene sulfonate at various temperatures, J. Dispers. Sci. Technol. 38 (11) (2017) 1625–1632, https://doi.org/10.1080/01932691.2016.1269650.
[30] K. Nakamura, T. Shikata, Threadlike micelle formation of anionic surfactants in aqueous solution, Langmuir 22 (24) (2006) 9853–9859, https://doi.org/10.1021/la061031w.
[31] S.K. Ghosh, V. Rathee, R. Krishnaswamy, V.A. Raghunathan, A.K. Sood, Re-entrant phase behavior of a concentrated anionic surfactant system with strongly binding counterions, Langmuir 25 (15) (2009) 8497–8506, https://doi.org/10.1021/la804330x.
[32] S.P. Gupta, Studies on novel phase behavior of ionic amphiphile-water systems, Thesis, 2014.
[33] W. Helfrich, Defect model of the smectic a-nematic phase transition, J. Phys. France 39 (11) (1978) 1199–1208, https://doi.org/10.1051/jphys:0197800390110119900.
[34] R. Holyst, Dislocation loops in finite systems, Phys. Rev. B 50 (1994) 12398, https://doi.org/10.1103/PhysRevB.50.12398.
[35] D.J. Mitchell, B.W. Ninham, Curvature elasticity of charged membranes, Langmuir 5 (4) (1989) 1121–1123, https://doi.org/10.1021/la00088a044.
[36] R. Beck, H. Hoffmann, Phase behaviour and physical properties of mixtures of calcium salts of alpha - sulfonated fatty acid methyl ester and a cosurfactant, Phys. Chem. Chem. Phys. 3 (2001) 5438–5443, https://doi.org/10.1039/B106516P.
[37] R. Beck, Y. Abe, T. Terabayashi, H. Hoffmann, A novel l3-phase from a ca-salt of an anionic surfactant and a cosurfactant, J. Phys. Chem. B 106 (13) (2002) 3335–3338, https://doi.org/10.1021/jp0125911.
[38] D.J. Mitchell, G.J.D. Tiddy, L. Waring, T. Bostock, M.P. McDonald, Phase behaviour of polyoxyethylene surfactants with water. Mesophase structures and partial miscibility (cloud points), J. Chem. Soc. Faraday Trans. I 79 (1983) 975–1000, https://doi.org/10.1039/F19837900975.
[39] M. Jonstromer, R. Strey, Nonionic bilayers in dilute solutions: effect of additives, J. Phys. Chem. 96 (14) (1992) 5993–6000, https://doi.org/10.1021/j100193a064.
[40] C.A. Miller, M. Gradzielski, H. Hoffmann, U. Kramer, C. Thunig, Experimental results for the l3 phase in a zwitterionic surfactant system and their implications regarding structures, Colloid Polym. Sci. 268 (1990) 1066–1072, https://doi.org/10.1007/BF01410596.
[41] M. Bergmeier, H. Hoffmann, F. Witte, S. Zourab, Vesicles from single-chain hydrocarbon surfactants and perfluoro cosurfactants, J. Colloid Interface Sci. 203 (1) (1998) 1–15, https://doi.org/10.1006/jcis.1998.5486.
[42] M. Cates, D. Roux, D. Andelman, S.C. Milner, S. Safran, Random surface model for the l3-phase of dilute surfactant solutions, Europhys. Lett. 5 (8) (1988) 733–739, https://doi.org/10.1209/0295-5075/5/8/012.
[43] G. Porte, P. Bassereau, J. Marignan, J. May, Shape transformations of the aggregates in dilute surfactant solutions: a small-angle neutron scattering study, J. Phys. France 49 (1988) 511–519, https://doi.org/10.1051/jphys:01988004903051100.
[44] S.P. Gupta, M. Thomas, A. Chowdhury, V.A. Raghunathan, Effect of adsorbed polyelectrolytes on the interactions and elasticity of charged surfactant bilayers, J. Phys. Condens. Matter 32 (2020) 194004, https://doi.org/10.1088/1361-648X/ab6d8d.